Available online at www.sciencedirect.com
ScienceDirect
Catalysis Communications 8 (2007) 410–415
CATALYSIS COMMUNICATIONS
www.elsevier.com/locate/catcom

The Ba-hexaaluminate doped with CeO_2 nanoparticles for catalytic combustion of methane

Shunqing Li [a,b], Xiaolai Wang [a,*]

[a] State Key Laboratory for Oxo Synthesis and Selective Oxidation, Lanzhou Institute of Chemical Physics, Chinese Academy of Sciences, Lanzhou 730000, PR China

[b] The Graduate University of the Chinese Academy of Sciences, Beijing 10039, PR China

Received 17 August 2005; received in revised form 14 June 2006; accepted 10 July 2006
Available online 15 July 2006

Abstract

The Ba-hexaaluminate doped with CeO_2 nanoparticles with high surface area for catalytic combustion have been prepared by using the alumina sol as the $(NH_4)_2CO_3$ coprecipitation precursor and supercritical drying method. The catalysts are composed of the rod-like particles and granular ones. The $CeO_2/BaAl_{12}O_{19-\alpha}$ catalyst possesses the highest surface area (83.5 m^2/g) and the smallest CeO_2 mean crystallite size (24.3 nm). Introduction of transition metal ion into the Al_2O_3 spinel leads to the increase of the catalytic activity. Nevertheless the hexaaluminate cannot be obtained when further increasing the introduction, the components of the main crystalline phases are $Al_{2.267}O_4$ and CeO_2. The $CeO_2/BaFeMnAl_{10}O_{19-\alpha}$ catalyst possesses the lowest complete conversion of methane temperature, probably due to the high surface area and the excellent performance of activating oxygen.

Keywords: Hexaaluminate; Catalytic combustion; Methane; CeO_2 nanoparticles

1. Introduction

Catalytic combustion has many advantages over conventional flame combustion in supressing NO_x emission and in improving energy efficiency simultaneously [1–3]. Ba-substituted hexaaluminates (BHA) are considered suitable catalysts due to their high thermal stability and good combustion activity [4–6]. Since Zarur et al. [7,8] prepared hexaaluminate nanoparticles with high catalytic activities by adopting reverse microemulsion-mediated synthesis method, many efforts have been made to increase the catalytic activity and improve the thermal stability of the catalyst [9,10]. Further improvement of the performance of the catalysts is quite necessary.

Cerium oxide has been employed extensively as a catalyst or as a textural and structural promoter for supported metal or metal oxide catalysts. Generally, the structural promotion effect is attributed to the cerium capability of forming crystalline oxides with lattice defects which may act as catalytic active sites [11], whereas its textural promotion effect is given by the excellent thermal and mechanical resistance which CeO_2 confers to catalysts [12–15]. An interesting property of CeO_2 is its ability to release and absorb oxygen during alternating re-dox conditions, and hence to function as oxygen buffer. As a part of car exhaust gas clean up catalysts, CeO_2 widens the "lambda window" in which the catalyst can simultaneously catalyze the reduction of NO and the oxidation of CO and hydrocarbons [16,17]. Therefore, CeO_2 as the additive of hexaaluminate probably improve the performance of combustion catalyst due to the mutual influence between CeO_2 and Ba-hexaaluminates [7,18].

In this work, the Ba-hexaaluminates doped with CeO_2 nanoparticles were prepared and the catalytic activities for methane combustion were investigated. Moreover, N_2-adsorption, X-ray diffraction (XRD), TEM, temperature programmed reduction (TPR) of hydrogen and tem-

* Corresponding author. Tel.: +86 931 8275727; fax: +86 931 8277787.
E-mail address: lishunqing2003@yahoo.com.cn (X. Wang).

1566-7367/$ - see front matter © 2006 Elsevier B.V. All rights reserved.
doi:10.1016/j.catcom.2006.07.011

perature programmed desorption (TPD) of oxygen were used to study the structural and morphological properties.

2. Experimental

2.1. Preparation of the catalysts [19,20]

The mixed appropriate amounts of transition metal, cerium, barium nitrates and alumina sol solution was poured into a well-stirred container with an ammonium carbonate solution at 60 °C to form the precursor precipitate. The mol ratio (the nominal one) of CeO_2 and hexaluminate type phase was 1:1 and the mol ratio of transition metal, barium nitrates and alumina sol solution was calculated by the molecular formula of hexaaluminate. The slurry was aged for 10 h at 60 °C, and then filtered, washed with distilled water. The filter cake was then dried under supercritical conditions of ethanol (260 °C, 8.0 MPa). Finally, the aerogel was calcined in a muffled furnace at 1200 °C for 5 h in air.

2.2. Catalyst characterization

The surface area and the pore size distribution of the different catalysts were determined by nitrogen adsorption at 77 K on a Micrometrics ASAP 2010 instrument. The surface area was determined according to the Brunauer–Emmett–Teller theory and the analysis of the diameter and the pore volume were carried out according to BJH equation.

The crystal phases of the various catalysts were detected by X-ray diffraction, on a Shimadzu Diffractometer XD-3A. The operation parameters were: Cu Kα radiation, Ni filter, 30 mA, 40 kV, 2θ scanning from 5 °C to 80 °C with the scanning speed of 4°/min. The mean crystallite size $\bar{d}$ of CeO_2 particles was determined from XRD line broadening measurements using the Scherrer equation: $\bar{d} = k\lambda/\beta\cos\theta$, where λ is the X-ray wave length ($\lambda = 1.5418$Å), k is the particle shape factor, taken as 0.9 for cubic particles, β is the full width at half maximum of the CeO_2 (1 1 1) line (in radians), and θ is the diffraction angle [21,22].

The morphology and size of the catalysts were studied using transmission electron microscopy (JEOL, JEM-2000FX) with a voltage of 200 kV. The test samples were prepared by its suspension on the copper net.

Temperature programmed desorption (TPD) of O_2 and temperature-programmed reduction (TPR) with H_2 were performed using a GC 7890 IIgas chromatograph equipped with a TCD. The sample (50 mg) was preheated in flowing air at 800 °C for 1 h before each TPD or TPR test. In TPR analyses a 10 vol % H_2/Ar mixture (35 cm^3 min^{-1}) was used to reduce the sample by heating 10 °C min^{-1} up to 900 °C. Water produced by the sample reduction was removed by using 5 Å molecular sieve as the desiccant before reaching the detectors. In O_2 TPD analyses the sample was heated 10 °C min^{-1} up to 900 °C in flowing He (35 cm^3 min^{-1}).

2.3. Activity tests

The reaction of methane combustion was carried out in a conventional flow system under atmospheric pressure. Catalyst (0.8 ml) (20–40 mesh) was loaded in a quartz reactor (i.d. 10 mm), with quartz fiber packed at the end of the catalyst bed. A mixture gas of 4 vol % O_2 and 1 vol% CH_4 (nitrogen as balance) was fed into the catalyst bed at GHSV = 15,000 h^{-1}. The main products are carbon dioxide and water. The compositions of the inlet and dehydrated outlet gas were analyzed by an on-line gas chromatography with a packed carbon molecular sieve column and a thermal conductivity detector.

3. Results and discussion

3.1. Surface area and pore size distribution

The reaction of catalytic combustion at high temperatures is limited by the mass transfer of reactants to the catalyst surface from the gas phase. Maintaining large surface area and pore structure of combustion catalysts is important in promoting the reaction under the mass transfer limitation. The surface area and pore volume as well as average pore diameter of Ba-hexaaluminate catalysts doped with CeO_2 nanoparticles are summarized in Table 1. The catalysts with high surface area in the range between 48 and 84 m^2/g are obtained. The $CeO_2/BaAl_{12}O_{19-\alpha}$ catalyst possesses the highest surface area and the surface area decreases with substitution of Mn ions. The trend of the variation of pore volume is identical to that of surface area, showing the structure of pore plays an important role in determining the surface area of the catalyst. Nevertheless the $CeO_2/BaFeMnAl_{10}O_{19-\alpha}$ catalyst possesses high surface area due to the formation of macropore. The pore diameters varies from 68 to 110 Å, showing the introduction of transition metal ions into the Al_2O_3 spinel has some effect on the structure of pores. Compared with those reported in literature [19], the catalysts in a low pore to crystal size ratio are obtained herein. The possible reason is given as following: Since the alumina network forms by using the alumina sol as the co-precipitation precursor before the co-precipitation and the network structure is effectively maintained by using SCD method, the network of the aerogel has a higher stability and more compact structure than that formed by using aluminum nitrate, leading to the decrease in the mobility of aluminum at high temperature. As a result, the growth of crystal is effectively suppressed and the structure of pore is also effectively maintained.

3.2. Crystalline phases

The XRD patterns of the catalysts are shown in Fig. 1. The hexaaluminate and CeO_2 phases are obtained for the $CeO_2/BaAl_{12}O_{19-\alpha}$ catalyst and the $CeO_2/BaMnAl_{11}O_{19-\alpha}$ catalyst; meanwhile the introduction of Mn into the Al_2O_3

Table 1
Properties of the catalysts

Catalyst	S_{BET} (m^2/g)	V_{pore} (cm^3/g)	d_{pore} (Å)	$\bar{d}_{CeO_2}(111)$nm
$CeO_2/BaAl_{12}O_{19-\alpha}$	83.5	0.166	79.6	24.3
$CeO_2/BaMnAl_{11}O_{19-\alpha}$	55.9	0.118	84.4	34.7
$CeO_2/BaMn_2Al_{10}O_{19-\alpha}$	47.8	0.080	67.2	48.5
$CeO_2/BaFeMnAl_{10}O_{19-\alpha}$	75.3	0.206	109.3	40.5

spinel leads to the increase of α-Al_2O_3 phase. Nevertheless the hexaaluminate cannot be obtained when further increasing the introduction, the components of the main crystalline phases are $Al_{2.267}O_4$ [JCPDS 80-1385] and CeO_2, meanwhile the transition metal oxides and barium oxide cannot be observed, indicating that the introduction of transition metal ions into the Al_2O_3 spinel is complete and barium oxide is highly dispersed. In addition, the results in Table 1 reveal that CeO_2 particles with small size in the range between 25 and 50 nm are obtained and the mean crystallite size increases with the introduction of transition metal ions into the Al_2O_3 spinel. It is referred that the mobility of Ce^{4+} ions increases with the further introduction, which cause the growth of CeO_2 crystal.

3.3. Morphology of catalysts

Fig. 2 presents the TEM results of the catalyst. The result reveals that the samples are composed of the rod-like particles and granular ones. Combined with the XRD analysis, the former corresponds to the hexaaluminate and $Al_{2.267}O_4$ crystals of 50–150 nm in length and 5–20 nm in diameter, which shows the anisotropy crystal growth. The latter correspond to CeO_2 particles, the size of which distributes in the range of 10–35 nm. The results are consistent with the BET analysis; the catalysts with high surface area are obtained due to the small crystalline sizes. Moreover rod-like hexaaluminate is most effective in retarding sintering because of the small number of contact points between the particles [21,22]. Meanwhile, The TEM observation shows the mean crystallite size of CeO_2 particles increases with further introduction of the transition metal ion into Al_2O_3 spinel, which is identical to the XRD analysis. It is worthwhile to note that some CeO_2 particles adhere to the surface of the hexaaluminate and $Al_{2.267}O_4$ crystal, which probably suppresses the growth of CeO_2 particles and improves thermal stability of the catalyst.

3.4. TPR measurements

TPR under hydrogen is used to evaluate the reducibility of the metal ions introduced in the barium hexaaluminate structure [23]. The TPR profiles of the catalysts are shown in Fig. 3. Two main reduction peaks around 350 °C and 800 °C are present for the $CeO_2/BaAl_{12}O_{19-\alpha}$ catalyst. The first one, probably, corresponds to the removal of surface oxygen, while the latter to bulk oxygen from CeO_2 structure [24]. Meanwhile two main reduction peaks are present with the introduction of the transition metal ions. The reduction peak appearing at lower temperature probably corresponds to the most reactive species [6], which can be attributed to the co-reduction of the transition metal ions and surface oxygen from CeO_2 structure. When compared to the temperature of maximal consumption of hydrogen (T_{max}) between the $CeO_2/BaAl_{12}O_{19-\alpha}$ catalyst

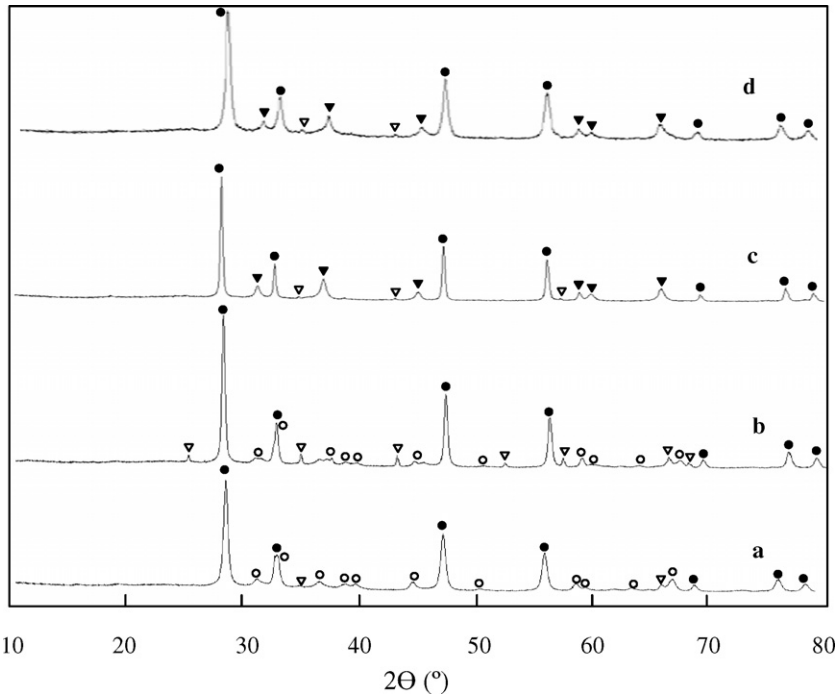

Fig. 1. XRD patterns of the catalysts: (a) $CeO_2/BaAl_{12}O_{19-\alpha}$; (b) $CeO_2/BaMnAl_{11}O_{19-\alpha}$; (c) $CeO_2/BaMn_2Al_{10}O_{19-\alpha}$; (d) $CeO_2/BaFeMnAl_{10}O_{19-\alpha}$; (●) CeO_2; (○) $Ba_{0.717}Al_{11}O_{17.282}$; (▽) α-$Al_2O_3$; (▼) $Al_{2.667}O_4$.

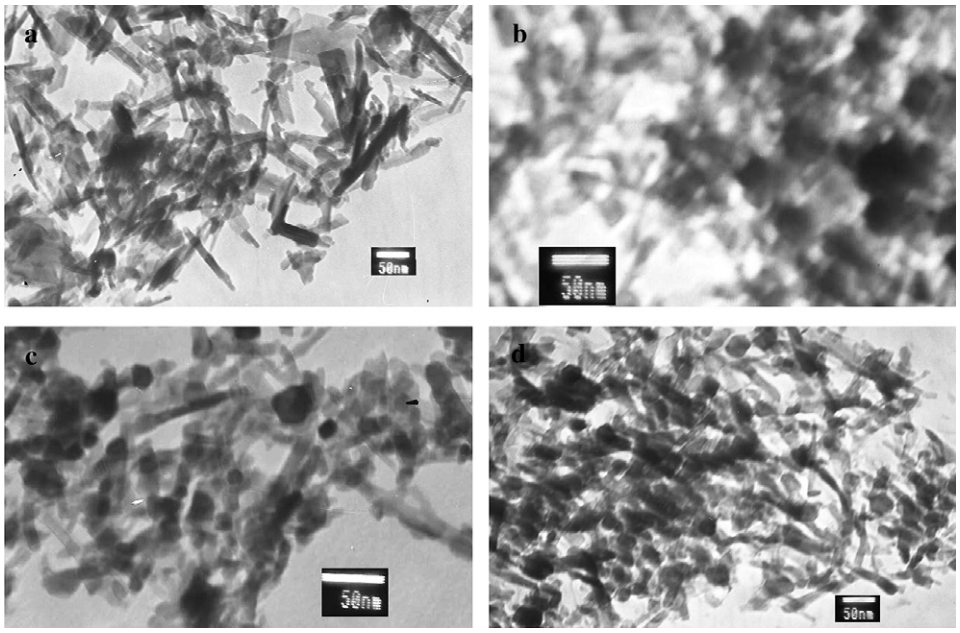

Fig. 2. TEM photographs of the catalysts: (a) $CeO_2/BaAl_{12}O_{19-\alpha}$; (b) $CeO_2/BaMnAl_{11}O_{19-\alpha}$; (c) $CeO_2/BaFeMnAl_{10}O_{19-\alpha}$ and (d) $CeO_2/BaMn_2Al_{10}O_{19-\alpha}$.

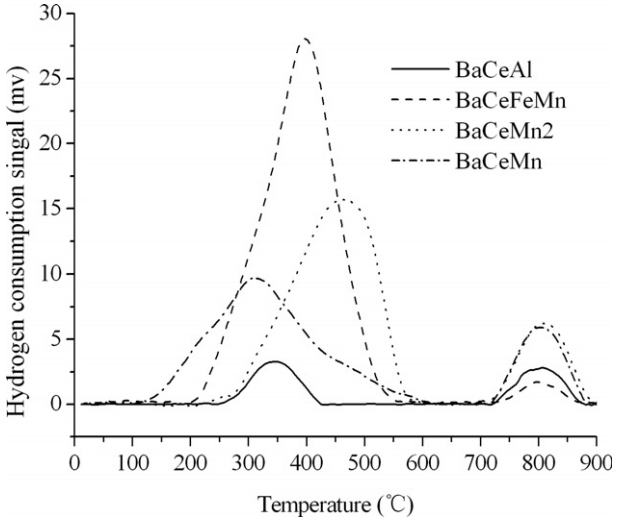

Fig. 3. TPR under hydrogen of the catalysts.

and the $CeO_2/BaMnAl_{11}O_{19-\alpha}$ catalyst, it decreases with the Mn ion substitution. Nevertheless, it increases with the further introduction probably due to the transformation of the crystalline phase. Since the hexaaluminate possesses the peculiar layered structure that consists of γ-Al_2O_3 spinel block intercalated by planes (mirror planes) in which the largest cations are located, Mn^{3+} are quite easily reduced by hydrogen diffusing quickly between the spinel blocks. While $Al_{2.267}O_4$ crystal possesses more compact structure (the face-centered cubic structure), Mn^{3+} are relative difficultly reduced. When compared to peak areas, the maximum is present for the $CeO_2/BaFeMnAl_{10}O_{19-\alpha}$ catalyst. Meanwhile, the temperatures required for the reduction of transition metal ions are high compared to the reduction of bulk oxides, indicating the ions enter the alumina lattice. The TPR results are consistent with those from XRD analysis.

3.5. O_2-TPD

Two different reaction mechanisms have been proposed for hexaaluminate involving two different oxygen species [5]. At low temperature an Eley–Rideal mechanism occurring between adsorbed oxygen and gaseous CH_4 has been assumed. At high temperature, when the coverage of molecular O_2 strongly decreases, lattice oxygen becomes active and the methane oxidation can be described by a redox mechanism. Hence, lattice oxygen species play an important role in the catalytic reaction at high temperature. TPD profiles of oxygen from the catalysts are shown

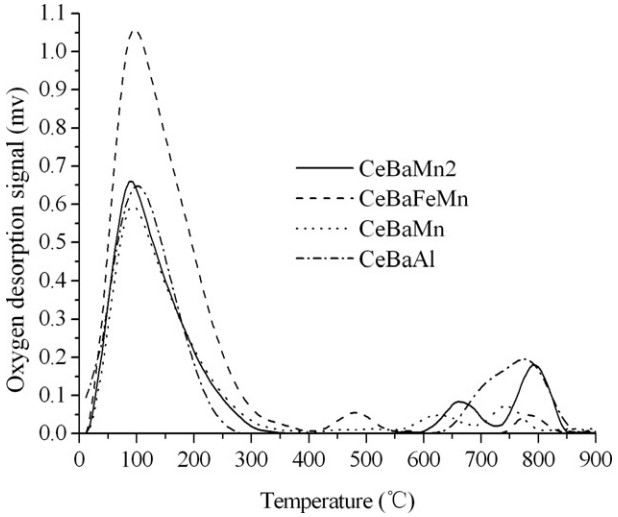

Fig. 4. TPD profiles of oxygen from the catalysts.

in Fig. 4. Two main reduction peaks around 150 °C and 750 °C are present. The first one, probably, corresponds to physically adsorbed oxygen on the on the catalyst surface, while the latter to the lattice oxygen. When compared to the peak position and area, the lowest temperature and maximum area are present for the $CeO_2/BaAl_{12}O_{19-\alpha}$ catalyst. The result reveals that the lower size of CeO_2 particles leads to more active oxygen spices and higher content of lattice oxygen, which is expected owing to the higher defectiveness [25–27]. Moreover, it is worthwhile to note that other small peaks between 400 °C and 700 °C are present, which probably corresponds to the lattice oxygen formed by the introduction of transition metal ion into the Al_2O_3 spinel. The peak at 500 °C is present for the $CeO_2/BaFeMnAl_{10}O_{19-\alpha}$ catalyst, indicating the catalyst possesses the most reactive lattice oxygen.

3.6. Catalytic combustion of methane

The catalytic activities for methane combustion over the catalysts are shown in Fig. 5. Meanwhile $T_{10\%}$, $T_{50\%}$ and $T_{90\%}$ corresponding to 10%, 50% and 90% conversion are reported in Table 2. $BaAl_{12}O_{19}$ catalyst is poorly active, the initial temperature of methane combustion. $T_{10\%}$ is 650 °C, meanwhile $T_{90\%}$, as an index of complete conversion of methane is 840 °C. Compared with the $BaAl_{12}O_{19}$ catalyst, The $CeO_2/BaAl_{12}O_{19-\alpha}$ catalyst possesses higher activity with T_{10} as 535 °C and $T_{90\%}$, as 690 °C. It is obvious that the catalytic activity increases due to the introduction of CeO_2 nanoparticles into hexaaluminate. Although Ce^{4+} cannot enter the hexaaluminate lattice, it acts as the active phase of the catalyst. The H_2-TPR and O_2-TPD results verify that the activity is closely related to the redox couple between Ce^{4+} and Ce^{3+} on the surface of CeO_2 particles. Nevertheless, the activity increases in a relatively low extent for the catalysts containing transition metal ion. For

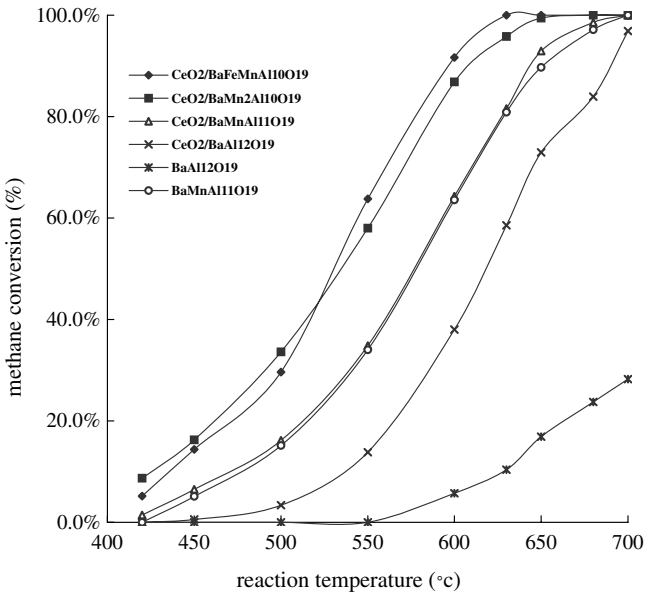

Fig. 5. Catalytic combustion of CH_4 over the catalysts.

Table 2
Catalytic activities expressed as $T_{10\%}$, $T_{50\%}$ and $T_{90\%}$ in °C

Catalysts	$T_{10\%}$ (°C)	$T_{50\%}$ (°C)	$T_{90\%}$ (°C)
$BaAl_{12}O_{19-\alpha}$	630	750	841
$BaMnAl_{11}O_{19-\alpha}$	470	580	655
$BaMn_2Al_{11}O_{19-\alpha}$	433	537	619
$CeO_2/BaAl_{12}O_{19-\alpha}$	535	618	690
$CeO_2/BaMnAl_{11}O_{19-\alpha}$	468	576	645
$CeO_2/BaMn_2Al_{10}O_{19-\alpha}$	426	534	611
$CeO_2/BaFeMnAl_{10}O_{19-\alpha}$	436	530	597

example, the $CeO_2/BaMnAl_{11}O_{19-\alpha}$ catalyst (T_{10} is 468 °C, T_{90} is 645 °C) has a slightly higher activity than the $BaMnAl_{11}O_{19-\alpha}$ catalyst (T_{10} is 470 °C, T_{90} is 655 °C). Since the mean crystallite size increases with the introduction of transition metal ions into the Al_2O_3 spinel, the content of Ce species on the surface of CeO_2 particles decreases, causing the lower catalytic activity. The TPR results show that hexaluminate phases containing transition metal ions are mainly responsible for the activity [5]. In addition, the lowest ignition temperature ($T_{10\%}$) is obtained for the $CeO_2/BaMn_2Al_{10}O_{19-\alpha}$ catalyst and the lowest complete conversion of methane temperature ($T_{90\%}$) is obtained for the $CeO_2/BaFeMnAl_{10}O_{19-\alpha}$ catalyst owing to the excellent performance of activating oxygen.

4. Conclusions

CeO_2 as additive of hexaaluminate can improve performance of combustion catalyst, the effect of which is closely related to the mean size of CeO_2 nanoparticles. The Ba-hexaaluminate doped with CeO_2 nanoparticles with high surface area have been prepared by using the alumina sol as the $(NH_4)_2CO_3$ coprecipitation precursor and supercritical drying (SCD) method. The $CeO_2/BaAl_{12}O_{19-\alpha}$ catalyst possesses the highest surface area (83.5 m^2/g) and the smallest CeO_2 mean crystallite size (24.3 nm). Introduction of transition metal ion into the Al_2O_3 spinel leads to the increase of the catalytic activity. The $CeO_2/BaFeMnAl_{10}O_{19-\alpha}$ catalyst possesses the lowest complete conversion of methane temperature, probably due to the high surface area and the excellent performance of activating oxygen.

References

[1] D.L. Trimm, Appl. Catal. 7 (1983) 249.
[2] R. Prasad, L.A. Kennedy, E. Ruckenstein, Catal. Rev.-Sci. Eng. 26 (1984) 1.
[3] L.D. Pfefferle, W.C. Pfefferle, Catal. Rev.-Sci. Eng. 29 (1987) 219.
[4] M. Machida, K. Eguchi, H. Arai, J. Catal. 103 (1987) 385.
[5] M. Machida, K. Eguchi, H. Arai, J. Catal. 120 (1989) 377.
[6] P. Artizzu-Duart, J.M. Millet, N. Guilhaume, E. Garbowski, M. Primet, Catal. Today 59 (2000) 163.
[7] A.J. Zarur, J.Y. Ying, Nature 403 (2000) 65.
[8] A.J. Zarur, H.H. Hwu, J.Y. Ying, Langmuir 16 (2000) 3042.
[9] PrashantK. Sahu, B.D. Kulkarni, R.B. Khomane, S.A. Pardhy, U.D. Phalgune, P. Rajmohanan, Renu Pasricha, Chem. Commun. 15 (2003) 1876.

[10] Fei Teng, Jinguang Xu, Zhijian Tian, Junwei Wang, Yunpeng Xu, Zhusheng Xu, Guoxing Xiong, Liwu Lin, Chem. Commun. 16 (2004) 1858.
[11] A. Trovarelli, Catal. Rev. -Sci. Eng. 38 (1996) 439.
[12] Y.F. Yu-Yao, J.T. Kummer, J. Catal. 106 (1987) 307.
[13] H.C. Yao, Y.F. Yu-Yao, J. Catal. 86 (1984) 254–265.
[14] T. Bunluesin, R.J. Gorte, G.W. Graham, Appl. Catal. B 14 (1997) 105.
[15] G.W. Graham, H.-W. Jen, R.W. McCabe, Catal. Lett. 44 (1997) 185.
[16] T. Kreuzer, E.S. Lox, D. Lindner, J. Leyrer, Catal. Today 29 (1996) 17.
[17] R.M. Heck, R.J. Farrauto, Catalytic Air Pollution Control – Commercial Technology, Van Nostrand, New York, 1995.
[18] Fei Teng, Ping Xu, Zhijian Tian, Guoxing Xiong, Yunpeng Xu, Zhusheng Xu, Liwu Lin, Green Chem. 7 (2005) 493.
[19] Junwei Wang, Zhijian Tian, Jinguang Xu, Yunpeng Xu, Zhusheng Xu, Liwu Lin, Catal. Today 83 (2003) 213.
[20] G. Groppi, M. Bellotto, C. Cristiani, P. Forzatti, P.L. Villa, Appl. Catal. A 104 (1993) 101.
[21] H.P. Klug, L.E. Alexander, X-ray Diffraction Procedures for Polycrystalline and Amorphous Materials, 1st ed., Wiley, New York, 1954.
[22] H.Y. Zhu, J.D. Riches, J.C. Barry, Chem. Mater. 14 (2002) 2086.
[23] M.A. Zwinkels, S.G. Järås, P.G. Menon, T.A. Griffin, Catal. Rev.-Sci. Eng. 35 (1993) 319.
[24] Radu Craciun, Solid State Ionics 110 (1998) 83.
[25] A. Trovarelli, C. Leitenburg, G. Dolcetti, J.L. Lorca, J. Catal. 151 (1995) 111.
[26] M. Che, E. Giamello, in: B. Delmon, J.T. Yates (Eds.), Studies Surface Science and Catalyst, 57, 1990, p. 265.
[27] I-Pin Chen, Shiow-Shyung Lin, Ching-Huei Wang, Lizone Chang, Jing-Song Chang, Appl. Catal. B 50 (2004) 49.